Experimental and Numerical Investigation of Flow Phenomena in Nonisothermal, Variably Saturated Bentonite–Crushed Rock Mixtures

Irina Engelhardt,* Stefan Finsterle, and Cor Hofstee

ABSTRACT

Mixtures of sodium bentonite and crushed rock are being examined as components of the engineered barrier system in a geologic repository of high-level nuclear waste. Laboratory experiments were performed to determine the thermal and unsaturated hydraulic properties of bentonite–crushed diorite mixtures. Water-retention curves were obtained from conventional pressure cell and evaporation experiments. In addition, transient data from heating and gas injection experiments on laboratory columns were analyzed using inverse modeling techniques. Measured pressures, temperatures, and drained-water volumes were jointly inverted to estimate absolute permeability, thermal conductivity, specific heat, and capillary strength parameters. Simultaneous matching of all available data—specifically the gas breakthrough at the top of the column—proved difficult, pointing toward aspects of the experimental design and the conceptual model that need to be refined. The analysis of sensitivity coefficients and the correlation structure of the parameters revealed the importance of accurately capturing coupled thermal hydrological processes within the column as well as the details of the experimental apparatus, such as heat losses and storage of water and gas in the measuring burette. The parameters estimated using different experimental and analytical procedures were consistent with one another, providing backfill material properties useful for the simulation of gas- and heat-generating nuclear waste repositories.

The Äspö Hard Rock Laboratory in Sweden is an underground facility designed to develop and test methods related to the permanent disposal of high-level nuclear wastes in consolidated crystalline basement rock. The actual waste would be placed in canisters in vertical deposition holes. These canisters would have an outer, 10-cm-thick copper wall and an inner steel lining. They would be separated from the host rock by a buffer consisting of 100% bentonite. A bentonite–crushed rock mixture would be used as backfill material to seal man-made cavities such as drifts, shafts, and boreholes. The bentonite acts as a hydraulic, chemical, and mechanical protection zone around the canisters.

The buffer and backfill materials selected to protect six simulated canisters at the Äspö test site are subjected to various processes, schematically shown for one canister in Fig. 1. After the canisters have been emplaced, water imbibes into the partially saturated buffer and backfill from fractures in the surrounding host rock, causing the bentonite to swell, which reduces its hydraulic conductivity. Gas may be generated in the repository as a result of corrosion, radiolysis, and other processes. The low permeability of the bentonite and its generally high gas entry pressure may prevent gas from escaping, potentially yielding very high gas pressures within the repository. After exceeding the gas entry pressure, the outward moving gas front would displace the water in the bentonite.

While the mineralogical properties of pure bentonite have been studied extensively (see, e.g., Müller-Vonmoos and Kahr, 1983; Pusch et al., 1990), little information is available on a backfill material consisting of bentonite–crushed rock mixtures. Few experiments on the capillary pressure–saturation relationship of mixtures of bentonite and an aggregate component (such as sand or crushed rock) have been performed (Tang et al., 1997; Johannesson et al., 1999; Jockwer et al., 2000). The gas entry pressures reported in these studies ranged from 0.04 and 2.5 MPa. Moreover, these experiments were conducted at 20°C, limiting their applicability to nonisothermal conditions such as those encountered at the Äspö facility or in a heat-generating nuclear waste repository.

Therefore, the first objective of our experimental study was to obtain quantitative data on nonisothermal two-phase flow in a bentonite–crushed rock mixture. The second objective was to identify the constitutive relationship model based on the experimental data. Finally, the third objective was to examine the use of inverse modeling techniques as a means to obtain relevant parameters from transient heating and gas injection experiments.

MATERIALS AND METHODS

Bentonite, Crushed Rock, and Äspö Water

The properties of the water and backfill materials are listed in Tables 1 and 2. The backfill contains 30% (w/w) SPV Volclay, a sodium bentonite from Wyoming, and 70% (w/w) crushed diorite. The water solution exhibits a ionic composition similar to that of Äspö formation water (see Table 2).

The density and viscosity of the synthetic Äspö water were measured at atmospheric pressure for different temperatures using a pycnometer and an Ubbelohde viscosimeter, respectively. Measured densities and viscosities were compared with values obtained using the empirical equations of Chierici (1994) (see Fig. 2).

The surface tension of Äspö water was measured at 20°C using a ring tensiometer. The relationship of Poling et al. (2001) is used in this study as it reproduces the surface tension measured for Äspö water (see Fig. 3).

Experimental Determination of the Capillary Pressure–Saturation Relation

On a macroscopic scale, capillary pressure can be expressed as an empirical function of liquid saturation. A specially designed pressure cell (see Fig. 4) with a height of 3.7 cm, a diameter of 5.4 cm, and a sample volume of 84.3 cm^3 was con-

Irina Engelhardt, Federal Institute of Geosciences and Natural Research (BGR), D-30655, Hannover, Germany; Stefan Finsterle, Lawrence Berkeley National Laboratory (LBNL), University of California, Berkeley, CA 94720; and Cor Hofstee, Netherlands Institute of Applied Geosciences (TNO-NITG), 3508 TA Utrecht, Netherlands. Received 10 Oct. 2002. Original Research Paper. *Corresponding author (I.Engelhardt@bgr.de).

Published in Vadose Zone Journal 2:239–246 (2003).

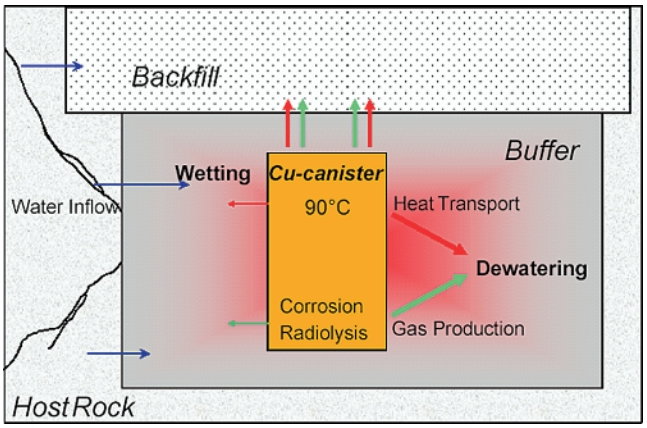

Fig. 1. Schematic of coupled thermal hydraulic processes at Äspö Hard Rock Laboratory.

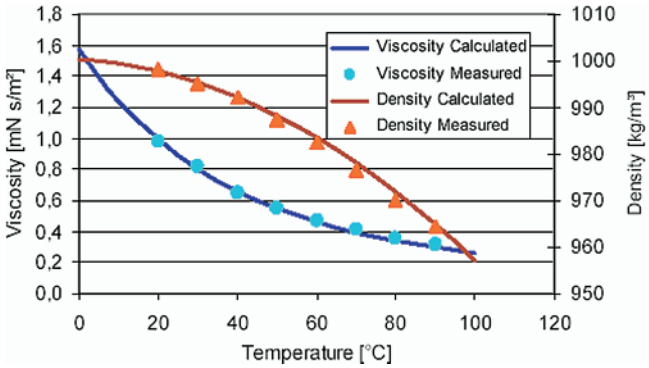

Fig. 2. Measured (symbols) and calculated (lines) viscosity and density of Äspö water as a function of temperature.

structed to determine capillary pressures in the range between 0 and 10 MPa (0–100 bar). The upper limit of 10 MPa (100 bar) is given by the entry pressure of the semipermeable cellulose membrane at the bottom of the pressure cell. Before packing the sample material into the pressure cell SPV Volclay and the crushed rock were added to Äspö water, minimizing potential air entrapment. The mixture was packed into the sample chamber to a dry density of 1.6 g cm^{-3}. A stepwise desaturation experiment was performed whereby 4 mL of water were extracted at each step, generating a drainage curve of the capillary pressure–saturation relationship. The entry pressure of the membrane was reached at a water saturation of approximately 40%, requiring the use of a different method to remove the water that is strongly adsorbed as a thin film to the surface of the clay crystals.

An alternative method involving a thermohygrometer was used to measure the capillary pressure >10 MPa (100 bar). Techniques involving drying of the sample in an oven to yield the drainage curve in the high suction range did not produce a homogeneous saturation distribution within the bentonite and destroyed many of its mineralogical properties. Synthetic Äspö water was added stepwise to an air-dry sample (thus yielding an imbibition curve) and allowed to equilibrate with the atmosphere inside a closed container (see Fig. 5). The relative humidity h in the container was measured and related to an equivalent capillary pressure according to Kelvin's equation:

$$P_{c,equ} = -\frac{RT}{M}\rho_w \ln(h) \qquad [1]$$

A complete list of symbols used in the equations and their definitions is given in the Appendix. Combining both pressure cell and thermohygrometer data seems appropriate as they reflect, respectively, the processes of capillary drainage in the wet range and removal of water through phase transition in the dry range.

The Brooks–Corey (Brooks and Corey, 1964) parameters λ, P_d, S_{wr}, and S_{nwr}, and van Genuchten (van Genuchten, 1980) parameters $n(m)$, α, S_{wr}, and S_{nwr} were determined by fitting these capillary pressure relations to the combined data from the pressure cell and thermohygrometer experiments. The consistency between the Brooks–Corey and van Genuchten parameters was examined by applying the following relationships proposed by Lenhard et al. (1989):

$$\lambda = \frac{m}{1-m}\left(1 - S_e^{1/m}\right) \qquad [2a]$$

with

$$S_e = \frac{S_w - S_{wr}}{1 - S_{wr}} \qquad [2b]$$

and

$$\alpha = \frac{S_x^{1/\lambda}}{P_d}\left(S_x^{-1/m} - 1\right)^{1-m} \qquad [3a]$$

with

$$S_x = 0.72 - 0.35\exp(-n^4) \qquad [3b]$$

Since surface tension decreases as temperature increases, capillary pressure is expected to be temperature dependent. Lenhard and Parker (1987) proposed to correct the capillary

Table 1. Properties of the backfill material used for the experiments.

Material	Parameter					
SPV Volclay†	Montmorillonite	Quartz	Feldspar	Specific density	Cation exchange capacity	Gravimetric water content
	%			g cm^{-3}	mol kg^{-1}	%
	75	15.2	5–8	2.76	0.76	8.5
Crushed diorite	6.3–3.5 mm		3.5–2 mm		< 2 mm	
	%					
	66		31		3	

† Müller-VonMoos & Kahr (1983).

Table 2. Composition of Äspö water.

Äspö Water	Parameter						
	Na^+	Mg^{2+}	Ca^{2+}	K^+	S^{2-}	Cl^-	pH
	mol L^{-1}						
	1.5×10^{-2}	2.7×10^{-3}	1.8×10^{-3}	3.6×10^{-4}	5.1×10^{-4}	1.9×10^{-2}	7.4

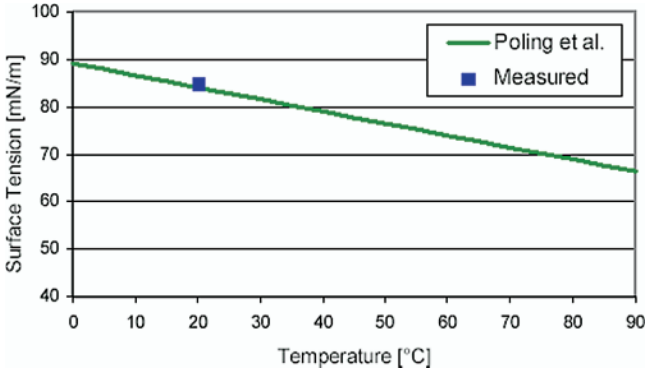

Fig. 3. Measured (square) and calculated (line) surface tension of Äspö water as a function of temperature.

pressure by a scaling factor β to account for the surface-tension dependence of capillary pressure. Noting the temperature dependence of surface tension, capillary pressures are scaled as follows:

$$P_{c,T} = P_{c,20}\beta \quad [4]$$

where

$$\beta = \frac{\sigma_T}{\sigma_{20}} \quad [5]$$

Here, σ_{20} is the surface tension at the reference temperature of 20°C prevailing during the pressure cell and thermohygrometer experiments.

Experimental Determination of Saturated Hydraulic Conductivity

The permeability was determined by applying a 2-MPa pressure difference over a 30-cm-long permeameter. The sample has a cross-sectional area of 19.6 cm^2. Three screens (metal, textile, and fine sand) at the bottom and top of the sample effect and facilitate one-dimensional flow in the permeameter.

Using the measured viscosity and density of Äspö water at 20°C and the measured volumetric flow rate Q into the burette, Darcy's Law was used to calculate the sample's permeability k:

$$k = -\frac{\mathbf{Q}}{A}\mu\left(\frac{1}{\nabla P_w - \rho\mathbf{g}}\right) \quad [6]$$

Saturated hydraulic conductivity at elevated temperatures was then calculated using the temperature dependence of viscosity and density (see Fig. 2):

$$K = k\frac{\rho g}{\mu} \quad [7]$$

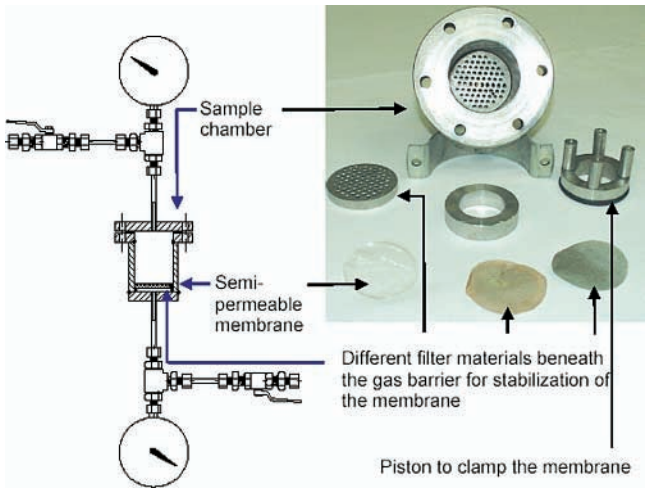

Fig. 4. Schematic drawing and parts of pressure cell apparatus.

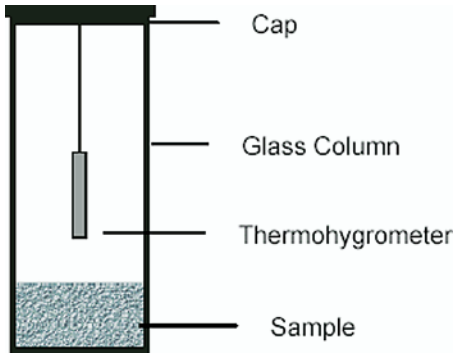

Fig. 5. Determination of the capillary pressure–saturation relationship based on vapor-pressure measurements using a thermohygrometer.

Column Experiments: Heating and Gas Injection

The permeameter described above was also used to study heat transfer and gas flow behavior within the backfill. A sample was pressurized to 1 MPa and then heated from below by maintaining a boundary temperature of approximately 90°C at the bottom of the column. Temperature was measured at five locations along the axis of the column (see Fig. 6). Heating was continued until a time-invariant temperature distribution was reached.

After the heating experiment, the experimental setup was reconfigured for the subsequent N_2 injection test. This involved replacing the water in the heating chamber with air, connecting the inlet to a pressurized N_2 source and the top of the column to a burette for outflow measurements. Reconfiguration of the experimental setup required approximately 10 min, during which heat input was interrupted. The sample and the burette were initially pressurized to 1 MPa. Nitrogen injection started with an applied pressure of 1.15 MPa, resulting in an inlet capillary pressure of 0.15 MPa. Subsequently, the injection pressure was increased stepwise to 1.5 and 2 MPa, displacing water from the sample into the burette. The gas in the burette was compressed, causing the pressure to increase, as displaced water and eventually N_2 gas entered the burette. Water discharge rate, gas pressure in the burette, and temperatures along the column were measured as a function of time and used as calibration data for inverse modeling; that is, thermal and hydraulic parameters were determined by automatically matching the calculated to the measured system behavior.

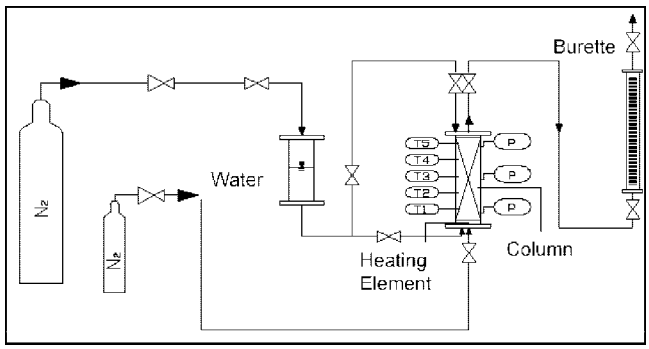

Fig. 6. Experimental setup for thermal and gas injection experiments (T1 through T5 indicate temperature sensors, P indicates a manometer).

Table 3. Material parameters and initial conditions of all model domains.

Parameter	Material				
	Backfill	Top	Bottom	Insulation	Burette
Porosity, %	48	1	95	0.1	95
Density, kg m^{-3}	2700	7800	7800	20	20
Permeability, m^2	8.6×10^{-19}	0.0	1.0×10^{-10}	0.0	1.0×10^{-10}
Heat cond., W m^{-1} K^{-1}	2.14	14.00	14.00	0.25	0.01
Spec. heat, J kg^{-1} K^{-1}	1020	460	460	2000	10
Relative permeability and capillary pressure functions					
van Genuchten model		Constant			
		$k_{rl} = 0$ $k_{rg} = 0$	$k_{rl} = 1$ $k_{rg} = 1$	$k_{rl} = 0$ $k_{rg} = 0$	$k_{rl} = 0$ $k_{rg} = 0$
S_{wr}	0.07	$P_c = 0$	$P_c = 0$	$P_c = 0$	$P_c = 0$
S_{nwr}	0.01				
n	1.44				
1/α, Pa	1.89×10^5				
Brooks–Corey model					
S_{wr}	0.07				
S_{nwr}	0.01				
λ	0.40				
P_d, Pa	1.1×10^5				

Model Development and Inverse Modeling Procedure

The TOUGH2 multiphase flow simulator (Pruess et al., 1999) was used to simulate the thermal and gas injection experiments. A one-dimensional, radially symmetric model was developed to simulate the experiment. The column was discretized in vertical direction into 60 0.5-cm-thick elements. Radial heat loss through the insulation was facilitated by adding a heat-conducting, hydraulically impermeable boundary element. A similar grid element was attached at the top of the column to account for heat storage in and heat losses through the end cap. Because the sensor measuring the heater temperature failed, the temperature of the lowest sensor (T1) was prescribed as a time-dependent Dirichlet boundary condition. This approach is also preferred because accurately capturing the heat transfer from the heater to the fluid, through the end cap, and into the sample would have introduced systematic errors and thus a bias in the estimation of thermal properties of the bentonite–crushed rock mixture. For the simulation of the N_2 injection experiment, the top element was connected to an element representing the burette. This element had the correct volume and initial gas saturation so that incoming liquid or N_2 would lead to an appropriate increase in pressure. The sample column itself was initialized as fully water saturated with a pressure of 1 MPa and a temperature of 19.4°C.

The thermal and gas-injection experiments were simulated in a single model run. The thermal experiment was started at a time −285 466 s (approximately −3.3 d) and continued to time zero. Next, a 600-s phase with no heat input was simulated, representing the approximate time needed to reconfigure the setup for the subsequent gas injection experiment. Heating was resumed, and gas was injected at prescribed pressures for approximately 16.9 d. Both the Brooks–Corey and van Genuchten models were used to describe the two-phase relative permeability and capillary pressure functions. The material parameters used for the bentonite–crushed rock mixture are given in Table 3.

The iTOUGH2 code (Finsterle, 1999) was used to analyze the experimental data and to estimate the thermal and hydraulic parameter values. iTOUGH2 provides inverse modeling capabilities for the TOUGH2 simulator. Thermal and hydraulic parameters for the backfill material were estimated by automatically fitting the numerical model described above to measured temperature, pressure, and water flow rate data.

To avoid overparameterization, the pore-size distribution indices λ and n as well as the residual saturations S_{wr} and S_{nwr} were fixed at the values determined from the pressure cell and thermohygrometer data, and only four parameters were estimated by inverse modeling: absolute permeability, gas entry pressure P_d (or capillary strength parameter 1/α), thermal conductivity, and the specific heat of the backfill material. Since both hydraulic parameters were expected to vary over many orders of magnitude, we estimated their logarithms. Adding more parameters yielded ill-posed inverse problems with nonunique solutions and high estimation uncertainties as a result of strong parameter correlations. The four selected parameters are those with the highest overall sensitivity that could be estimated relatively independently.

Since heat and fluid flow are coupled processes, any error in the hydraulic properties would lead to a bias in the thermal property estimates. To avoid this potential bias, thermal and hydrologic properties were determined simultaneously despite the fact the permeability and capillary strength parameters were available from the experiments described above.

RESULTS

Capillary Pressure Curve

The capillary pressure–saturation curve was determined over a wide range of saturations. Parameter values of the Brooks–Corey model (λ = 0.4, P_d = 0.11 MPa, S_{wr} = 0.07) and van Genuchten model (n = 1.44, 1/α = 0.189 MPa, S_{wr} = 0.07) were estimated by matching the pressure cell and thermohygrometer data. As shown in Fig. 7, both the Brooks–Corey and van Genuchten models represented the measured capillary pressure curves for intermediate saturations reasonably well. However, potentially significant deviations existed near full saturation and complete dryness. Equations [2] and [3] were used to convert the fitted Brooks–Corey parameters to equivalent van Genuchten parameters. This conversion was based on an average water saturation S_w of 0.5, as recommended by Lenhard et al. (1989). The resulting van Genuchten parameters were nearly identical to the parameter values estimated when matching the experimental data.

The relatively small value of the pore-size distribution

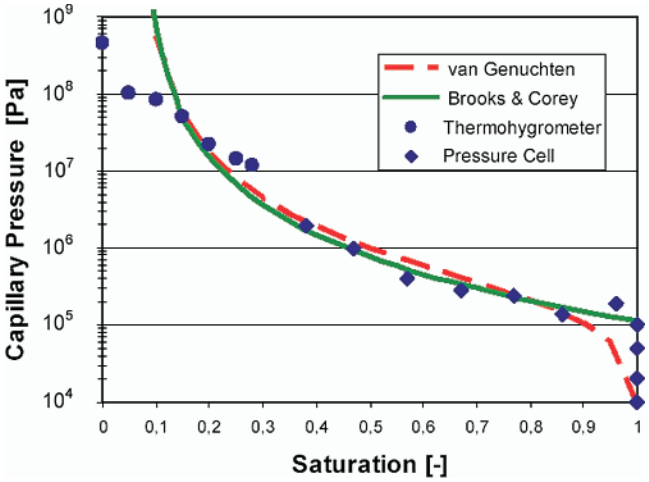

Fig. 7. Experimental capillary pressure–saturation data (symbols) and fitted Brooks–Corey and van Genuchten models (lines).

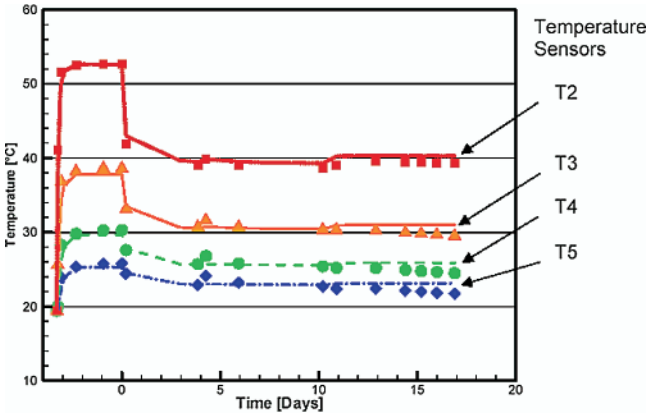

Fig. 8. Comparison between the measured (symbols) and calculated (lines) temperatures.

index indicated a wide range of pore sizes. This wide range of pore sizes may be attributed to a combination of features comprising the pore space. These include the roughness of the crushed rock, the development of clusters formed by coagulation, and possibly the bimodal nature of the mixture, resulting from pores between the bentonite and the crushed rock, pores between the clay aggregates, and pores between the montmorillonite crystals.

Employing Eq. [4] and [5], capillary pressures were reduced by about 20% as temperature increases from 20 to 90°C. The measured densities and viscosities of the Äspö formation water were used to account for the influence of temperature on the saturated hydraulic conductivity, which increased from 1.64×10^{-11} m s^{-1} at 20°C to 4.87×10^{-11} m s^{-1} at 90°C.

Estimation of Thermal and Hydraulic Parameter Values Using Inverse Modeling

Matching the simulated temperature, flow rate, and pressure data to the corresponding data from the column experiments yielded adequate estimates of thermal and hydraulic parameters. We first discuss the fit between the simulated and measured data.

Temperatures were well matched throughout the 3-wk experiment (see Fig. 8). During the heating phase, the temperature along the column was affected by heat conduction only; during the gas injection period, heat was transferred by both conduction and convection. The drop in temperature at time zero was a result of the 10-min interruption of heating during reconfiguration of the experimental setup. The temperature distribution simulated with the Brooks–Corey and van Genuchten models fit the measured profile equally well.

Figure 9 shows that the calibrated nonisothermal two-phase flow model with the van Genuchten functions provided a reasonably good fit to the measured amount of water collected in the burette during the gas injection experiment, especially at later times. However, during the first part of the gas injection experiment, both the van Genuchten and Brooks–Corey models significantly underestimated the displaced amount of water. The initial fast displacement of water seen in the data may be attributed to the possible presence of macropores, other fast-flow paths through the system, or short circuits in the packing of the permeameter. The macropores may arise from the card-house structure of flocculated sodium bentonite, with open pore space between clusters of randomly orientated individual particles (see Fig. 10).

After the entry pressure of the macropores was exceeded, a significant part of the pore space drained almost immediately, as seen after 4 d in the gas injection experiment (see Fig. 9). Micropores with a higher entry pressure subsequently drained at a slower rate. Neither the standard van Genuchten nor Brooks–Corey model exhibit a bimodal structure, and therefore an average curve was obtained as a result of the fitting process.

The distinct entry pressure of the Brooks–Corey model had a profound impact on the simulated system behavior. The Brooks-Corey model predicted that the N front penetrates the column to a distance of only 7.5 cm, with an almost piston-like displacement resulting in high gas saturations in the injection zone. The van Genuchten model, on the other hand, yielded a dis-

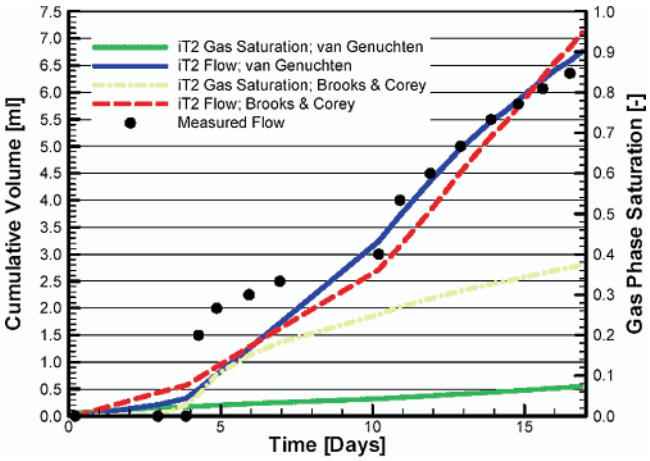

Fig. 9. Comparison of measured (circles) and calculated water flow (blue and red lines); calculated gas saturation 3 cm above the injection.

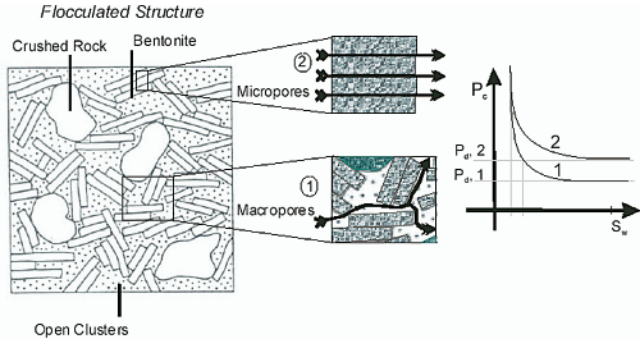

Fig. 10. Flocculated structure and flow paths in a bimodal medium: water moving through micropores and macropores.

persed gas distribution that reaches the top of the column after 10.8 d, with a relatively low maximum gas saturation of 28% near the injection point. The gas saturation 3 cm above the inlet is shown in Fig. 9.

Figure 11 shows the comparison between the pressure measured in the burette and the corresponding simulation result obtained with iTOUGH2. The initial, minor pressure increase resulted from displaced water entering the measuring device, thus slightly compressing the gas in the burette. The pressure increased much more rapidly as soon as the injected N_2 gas reached the top of the column. The van Genuchten model resulted in an early gas breakthrough at about 10.8 d, overestimating the late-time pressure in the burette. On the other hand, the Brooks–Corey model predicted a relatively sharp gas–liquid front within the column, preventing gas breakthrough. This yields a relatively good match to the observed pressures. No gas breakthrough was evident from the experimental data. The stepwise increase in the observed pressures was a result of the low manometer resolution of 0.01 MPa.

As discussed above, it appears that a secondary pore system with larger pore sizes affects flow near saturation. This behavior can be partially mimicked by a reduced Brooks–Corey entry pressure or by using the van

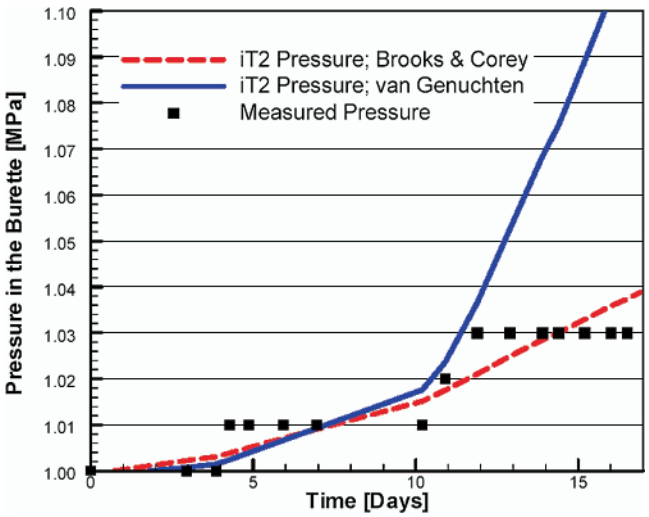

Fig. 11. Comparison of the measured (squares) and calculated pressure (lines) in the burette.

Table 4. Summary of the inverse modeling results.

Parameter	Model	Initial guess	Best estimate	σ_P	σ_P^*/σ_P
	van Genuchten		−17.89	0.02	0.40
log(k), m^2		−18.07			
	Brooks–Corey		−18.08	0.02	0.24
log(1/α), Pa	van Genuchten	5.28	5.15	0.14	0.40
log(P_d), Pa					
	Brooks–Corey	5.04	4.60	0.14	0.24
	van Genuchten		2.28	0.07	0.97
λ_T, W m^{-1} K^{-1}		2.14			
	Brooks–Corey		2.35	0.09	0.98
	van Genuchten		900	86.2	1.00
c, J kg^{-1} K^{-1}		1020			
	Brooks–Corey		900	99.6	1.00

Genuchten model, which allows water displacement for any non-zero capillary pressure. However, both models fail to reproduce early-time data, obtained soon after the start of the experiment. This suggests that constitutive relations derived from a bi- or multi-modal pore-size distribution such as those proposed by Durner et al. (1999) may yield better results, provided that the additional parameters required by these more sophisticated models can be identified and determined with acceptable estimation uncertainty.

Table 4 summarizes the best-estimate parameter sets obtained from the inversion. The absolute permeability corresponded well with the permeability determined by the standard permeameter method. Estimated thermal parameters (heat conductivity and specific heat) were in the range given by Kahr and Müller-Vonmoos (1982). The inversion of the data based on the van Genuchten model resulted in a 1/α value of 0.14 MPa at 90°C. The Brooks–Corey model yielded an entry pressure P_d of 0.04 MPa at 90°C. Even when corrected for temperature effects, this value was significantly lower than the 0.11 MPa obtained at 20°C using the pressure-cell and thermohygrometer data.

Sensitivity Analyses and Estimation Statistics

The statistical correlation coefficients of the estimated parameters were evaluated. In our inversion, permeability and the capillary strength parameter were highly correlated. The correlations among the parameters resulted in a conjoint impact of a parameter change on the system behavior. For the hydraulic parameters, this correlation means that the lower flux obtained by decreasing permeability can be partly compensated by decreasing the entry pressure P_d or capillary strength parameter 1/α. Since the thermal parameters were less correlated, the response of a change in thermal conductivity will not result in a significant variation of specific heat.

iTOUGH2 also calculates the ratio of the conditional estimation uncertainty σ^*_P and the marginal estimation uncertainty σ_P, which can be interpreted as an overall measure of how independently a parameter can be estimated (Finsterle, 1999). This ratio was small for the permeability and gas entry pressure, especially in the Brooks–Corey model, indicating that these parameters were generally highly correlated (see Table 4). Never-

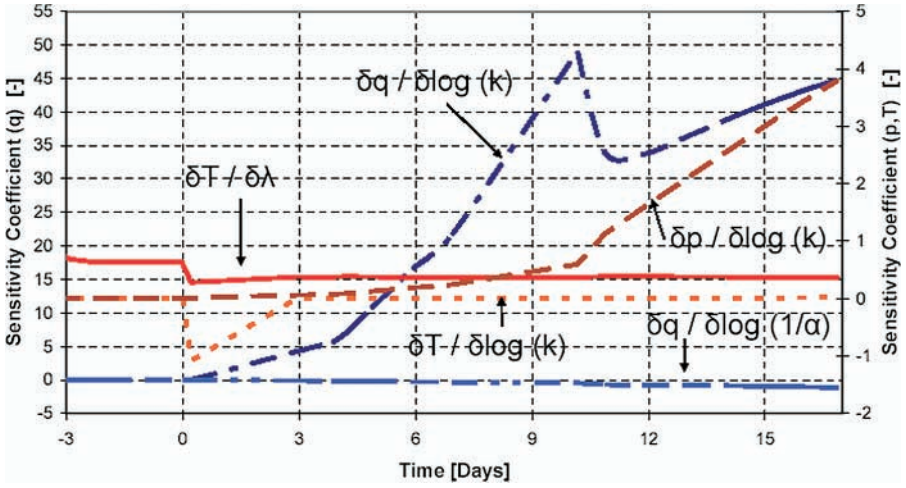

Fig. 12. Sensitivity of water flow, temperature at sensor T2, and gas pressure in the burette for the van Genuchten model.

theless, their high sensitivity yielded reasonably low estimation uncertainties.

Figure 12 shows the sensitivity coefficients of temperature T at sensor T2, flow rate q, and pressure p in the burette with respect to permeability $\log(k)$, the capillary strength parameter $\log(1/\alpha)$, and heat conductivity λ_T. The sensitivity analysis showed that the longer the experiment lasts, the more information about permeability and capillary strength can be drawn from the flow-rate data, as the sensitivity of both parameters continues to increase. At the time of gas breakthrough, the sensitivity of the water flow rate is at its maximum. Likewise, the sensitivity of the gas pressure in the burette increases rapidly after gas breakthrough. The sensitivity of temperature with respect to permeability was relatively small and approached zero as the test continued, indicating that the convective heat flow is less significant than the conductive heat transfer. However, the temperature data provided information about heat conductivity, particularly during the heating phase, as shown by the corresponding sensitivity curve.

SUMMARY AND CONCLUSIONS

The main objective of this study was to obtain experimental data that allow determination of thermal and two-phase flow parameters of bentonite–crushed rock mixtures under conditions representative of those at the Äspö Hard Rock Laboratory. In addition, we examined constitutive relationships suitable for predicting gas leakage from a gas-generating repository.

Flow-rate data and outlet pressure data in the compressed burette were difficult to match. This was most likely a result of the complex pore structure of the backfill material, which has a significant effect on gas flow behavior near full water saturation. The conventional Brooks–Corey and van Genuchten models are based on a unimodal pore-size distribution and therefore cannot account for the effect of macropores on multiphase flow in unsaturated backfill. Constitutive relationships derived from bimodal pore-size distributions (e.g., Durner et al., 1999) are expected to better capture the water displacement process in backfill materials near gas-generating nuclear waste canisters.

Inversion of the data from the gas injection experiment employing the van Genuchten function yields a capillary strength parameter $1/\alpha$ of 0.14 MPa at 90°C. This is consistent with the value of 0.19 MPa determined using a pressure cell and thermohygrometer experiments at 20°C.

Moreover, the relatively low entry pressure of the backfill material, determined with two different experimental techniques (conventional pressure cell measurements and the joint inversion of various transient data from column experiments) indicated that corrosion gas may penetrate the backfill material relatively easily, avoiding excessive pressure buildups in the repository, but increasing the risk of displacing contaminated pore water or radioactive gases.

We suggest performing sensitivity analyses and synthetic inversions to support the design of nonisothermal two-phase flow experiments by identifying data type, duration of experiments, measurement locations, and the accuracy required to extract the information necessary for estimating the parameters of interest.

ACKNOWLEDGMENTS

This work was supported by the Federal Institute of Geosciences and Natural Research (BGR), Hannover, Germany, the University of Tübingen, Center for Applied Geosciences (ZAG), Tübingen, Germany, and in part by the U.S. Department of Energy under Contract no. DE-AC03-76SF00098. Thanks to O. Trötschler, K. Emmerich and O. Kolditz for their scientific and technical support. We are very grateful for the suggestions and comments of the anonymous reviewers.

APPENDIX

Nomenclature

A	cross-sectional area of column (m^2)
c	specific heat ($J\ kg^{-1}\ K^{-1}$)
$\mathbf{g}$	vector of gravitational acceleration ($m\ s^{-2}$)
h	relative humidity
K	saturated hydraulic conductivity ($m\ s^{-1}$)
k	absolute permeability (m^2)

m, n van Genuchten model parameters, where $m = 1 - 1/n$
M molar mass of water (kg mol^{-1})
P_c capillary pressure (Pa)
$P_{c,20}$ capillary pressure (Pa) at reference temperature of 20°C
$P_{c,T}$ capillary pressure (Pa) at a given temperature T
P_d gas entry pressure (Pa)
P_{nw} pressure of the nonwetting fluid (Pa)
P_w pressure of the wetting fluid (Pa)
$\mathbf{Q}$ volumetric flow rate (m^3 s^{-1})
R universal gas constant (J mol^{-1} K^{-1})
S_e effective water saturation
S_{nwr} residual saturation of the nonwetting fluid
S_w saturation of the wetting fluid
S_{wr} residual saturation of the wetting fluid
T temperature (°C)
α van Genuchten capillary strength parameter (Pa^{-1})
β factor to correct capillary pressure for nonisothermal effects
λ pore-size distribution index of Brooks–Corey model
λ_T thermal conductivity (W m^{-1} K^{-1})
μ dynamic viscosity (N m^{-2} s)
ρ density (kg m^{-3})
σ surface tension (10^{-3} N m^{-1})
σ_{20} surface tension at reference temperature of 20°C (10^{-3} N m^{-1})
σ_P marginal estimation uncertainty
σ^*_P conditional estimation uncertainty
σ_T surface tension at a given temperature T (10^{-3} N m^{-1})

REFERENCES

Brooks, R.H., and A.T. Corey. 1964. Hydraulic properties of porous media. Hydrology Paper. 3. Colorado State Univ., Fort Collins, CO.

Chierici, G.L. 1994. Principles of petroleum reservoir engineering. Springer, Berlin.

Durner, W., E. Priesack, H.-J. Vogel, and T. Zurmühl. 1999. Determination of parameters for flexible hydraulic functions by inverse modeling. p. 817–829. *In* M.Th. van Genuchten et al. (ed.) Characterization and measurement of the hydraulic properties of unsaturated porous media. 2. Univ. of California, Riverside, CA.

Finsterle, S. 1999. iTOUGH2 user's guide. Report LBNL-40040. Lawrence Berkeley National Laboratory, Berkeley, CA.

Jockwer, N., R. Miehe, and I. Müller-Lyda. 2000. Untersuchung zum Zweiphasenfluss und diffusiven Transport in Tonbarrieren und Tongesteinen. (In German with English abstract). GRS-167. Braunschweig, Germany.

Johannesson, L.-E., L. Börgesson, and T. Sandèn. 1999. Backfill materials based on crushed rock. Clay Technology AB, Lund, Sweden.

Kahr, G., and M. Müller-von Moos. 1982. Wärmeleitfähigkeit von Bentonit MX80 und Montigel nach der Heizdrahtmethode. (In German with English abstract). NAGRA NTB 82-06. Wettingen, Switzerland.

Lenhard, R.J., and J.C. Parker. 1987. Measurement and predictions of saturation-pressure relationships in three-phase porous media systems. J. Contam. Hydrol. 1:407–424.

Lenhard, R.J., J.C. Parker, and S. Mishra. 1989. On the correspondence between Brooks–Corey and van Genuchten models. J. Irrig. Drain. Eng. 115:744–751.

Müller-Vonmoos, M., and G. Kahr. 1983. Mineralogische Untersuchungen von Wyoming Bentonit MX80 und Montigel. (In German with English abstract). NAGRA NTB 83–12. Wettingen, Switzerland.

Poling, B.E., and J.M. Prausnitz. and J.P. O'Connel. 2001. The properties of gases and liquids. 5th ed. McGraw-Hill, New York.

Pruess, K., C. Oldenburg, and G. Moridis. 1999. TOUGH2 user's guide. Version 2.0. Report LBNL-43134. Lawrence Berkeley National Laboratory, Berkeley, CA.

Pusch, R., O. Karnland, and H. Hökmark. 1990. GMM-A general microstructure model for qualitative and quantitative studies of smectite clay. SKB TR 90–43. Lund, Sweden.

Tang, X., J. Graham, and A.W. Wan. 1997. Measuring total suctions by psychrometers in triaxial tests. p. 213–216. *In* A.A. Balkema (ed.) Proceedings of the 14th International Conference on Soil Mechanics and Foundations Engineering. Vol. 1. 6–12 Sept. 1997. Hamburg, Germany.

van Genuchten, M.Th. 1980. A closed-form equation for predicting the hydraulic conductivity of unsaturated soils. Soil Sci. Soc. Am. J. 44:892–898.